catalysts

MDPI

Article

Ni-Al Self-Propagating High-Temperature Synthesis Catalysts in Dry Reforming of Methane to Hydrogen-Enriched Fuel Mixtures

Svetlana Tungatarova [1,2,*], Galina Xanthopoulou [3], George Vekinis [3], Konstantinos Karanasios [3], Tolkyn Baizhumanova [1,2], Manapkhan Zhumabek [1] and Marzhan Sadenova [4]

[1] D.V. Sokolsky Institute of Fuel, Catalysis and Electrochemistry, 142, Kunaev Str., Almaty 050010, Kazakhstan
[2] Department of Chemistry and Chemical Technology, Al-Farabi Kazakh National University, 71, Al-Farabi Str., Almaty 050040, Kazakhstan
[3] Institute of Nanoscience and Nanotechnology, NCSR Demokritos, Aghia Paraskevi, 15310 Athens, Greece
[4] Priority Department Centre "Veritas", D. Serikbayev East Kazakhstan State Technical University, 19, Serikbayev Str., Ust-Kamenogorsk 070000, Kazakhstan
* Correspondence: tungatarova58@mail.ru; Tel.: +7-727-291-6632

Abstract: The worldwide increase in demand for environmentally friendly energy has led to the intensification of work on the synthesis of H_2-containing fuel. The dry reforming of methane has become one of the most important avenues of research since the consumption of two greenhouse gases reduces the rate of global warming. A study of NiAl composite materials as catalysts for methane reforming has been carried out. Self-propagating high-temperature synthesis (SHS) has been used to produce NiAl catalysts. Comparative studies were carried out regarding the dry reforming and partial oxidation of methane, as well as catalysts prepared using the impregnation (IM) and SHS methods. A catalyst with 29% Ni and 51% Al after SHS contains the phases of NiAl and $NiAl_2O_4$, which are active phases in the dry reforming of methane. The optimal crystal lattice parameter (for the maximum possible conversion of CO_2 and CH_4) is 3.48–3.485 Å for Al_2O_3, which plays the role of a catalyst carrier, and 1.42 Å, for $NiAl_2O_4$, which plays the role of a catalyst. The aim of the work is to develop a new and efficient catalyst for the dry reforming of methane into a synthesis gas, which will further promote the organization of a new era of environmentally friendly energy-saving production methods.

Keywords: SHS combustion synthesis; catalyst; methane; dry reforming; partial oxidation

Citation: Tungatarova, S.; Xanthopoulou, G.; Vekinis, G.; Karanasios, K.; Baizhumanova, T.; Zhumabek, M.; Sadenova, M. Ni-Al Self-Propagating High-Temperature Synthesis Catalysts in Dry Reforming of Methane to Hydrogen-Enriched Fuel Mixtures. *Catalysts* **2022**, *12*, 1270. https://doi.org/10.3390/catal12101270

Academic Editors: Lei Liu and Zhijun Zuo

Received: 13 September 2022
Accepted: 13 October 2022
Published: 18 October 2022

1. Introduction

Population increase and economic growth have led to an increase in energy consumption [1]. Currently, all fossil fuels (natural gas, oil, and coal) are used to produce 70–80% of all generated energy [2]. Energy consumption results in significant carbon dioxide emissions, leading to environmental problems such as global warming and climate change [3,4]. The study of alternative and environmentally friendly systems has become the subject of public policy, including in the field of scientific research [5]. The problem of global warming is a serious challenge for the world. All leading countries have set themselves the goal of reducing their CO_2 emissions by 2030–2050. The conversion of methane, the main component of natural gas and biogas, into higher-value-added products is especially important [6–8]. Natural gas is a promising alternative to oil due to its huge reserves (198.8 trillion cubic meters) and the rapid development of technology [9,10]. The production of synthesis gas, which is the main base product in the chemical and petrochemical industries, is an important step in the conversion of natural gas. Methane is the simplest organic substance. The amount of CO_2 emitted by methane per unit of energy is lower than that of other hydrocarbon fuels. Therefore, it is a cleaner energy source that can

be used to replace fossil fuels and may also be one of the cheapest options for hydrogen production [11,12].

It is known that the dry reforming of methane (DRM) is one of the most promising technologies for the production of hydrogen-containing fuel compositions. Moreover, two greenhouse gases are utilized at once—methane and carbon dioxide, which contributes toward solving the problem of preserving the environment [13].

DRM has not yet been introduced into the industry, since this process has not yet been studied in enough depth. It is necessary to create more stable and selective catalysts for implementation [14]. Coke formation due to Boudouard, cracking, and reduction reactions is the main problem regarding the DRM [15]. Methane cracking is the main cause of carbon formation on nickel catalysts at high temperatures [16,17]. In this case, methane cracking is an endothermic reaction and proceeds at high temperatures, while the Boudouard reaction occurs at low temperatures. Therefore, it is recommended to use a nickel-based catalyst with supports having strong Lewis basicity [18].

The most commonly used catalyst preparation methods are coprecipitation [19], impregnation [20], sol-gel synthesis [21], and self-propagating high-temperature synthesis (SHS), including support on honeycomb block catalysts [22,23]. The method of preparation of these catalysts affects the dispersity, reducibility, and interaction between the active phases and support material, and also affects their catalytic characteristics [24].

SHS is an attractive method for the synthesis of advanced materials. This technique was discovered by scientists under the guidance of A.G. Merzhanov [25]. Combustion synthesis offers many advantages due to its short processing time, lower energy consumption and lower cost, and simple synthesis from cheap materials, which provides a more efficient way to produce refractory and hard materials [26,27]. The Indian scientists J.J. Kingsley and K.C. Patil proposed a new solution combustion synthesis (SCS) method [28], which can be used to obtain composite, porous ceramic materials and nanopowders [29]. They are widely used in gas sensors [30–33], as catalysts [34,35], and in electronics [36]. Products obtained by the SHS method are characterized by high purity and the ability to crystallize with clusters of nanosized material. Composition, uniformity, morphology, and stoichiometry can be precisely predetermined to obtain desired products that are highly crystalline and pure. SHS makes it possible to obtain not only nanomaterials and nanopowders but also structured catalysts, which have a thin film of catalytic material. This material can be applied easily to any ceramic or metal surface.

The relevance of DRM will only grow over time, due to the global trend of reducing greenhouse gas emissions. Supported nickel catalysts exhibit the highest activity in DRM. However, they have a significant drawback—the loss of process activity, due to coke formation. Various techniques are used to fight against this phenomenon.

Magnesium and aluminum oxides have proven in research to be suitable carriers. They are resistant to high temperatures and increase the stability of the catalyst by enhancing the nickel–carrier interaction and by forming a NiO–MgO solid solution and $NiAl_2O_4$/γ-Al_2O_4 spinel phases [37,38].

A study of the methane-reforming process was carried out using a Ni/Al_2O_3 catalyst [39]. It was found that methane conversion decreased with increasing pressure. The decrease was no more than 1–2%. González et al. [40] used Ni–Mg–Al hydrotalcites synthesized by the sol–gel method, with various Ni contents. These catalysts showed high activity and stability (CH_4 conversion was 98% for 8 h at 800 °C). Coke deposits were minimal on the catalyst containing 19 wt. % Ni.

The 5% Ni/Al_2O_3 catalyst was synthesized by SCS [41]. DRM was carried out in a flow quartz reactor at 500–900 °C. The initial CH_4:CO_2:Ar = 1:1:1 mixture was fed into the reactor at a space velocity of 60,000 h^{-1}. The nanocatalyst was selective with respect to CO and H_2. It showed fairly high stability, which persisted for 50 h. In contrast, the traditional Ni catalyst was subject to continuous deactivation. The high activity and selectivity of the nanocatalyst can be explained by the smaller particle size, better dispersion,

the stronger effects of interaction with the support, and the presence of reducible $NiAl_2O_4$ nanocrystallites.

It has been found that $NiAl_2O_4$ forming as a result of a chemical reaction is more coke-resistant than when it forms as a result of deposition [42,43]. The Ni/MgO catalyst is preferred over Ni/Al_2O_3, due to the low amount of carbon generated as a result of the formation of a NiMgO solid solution. In this case, the Boudouard reaction is inhibited [44]. CeO_2 stabilizes tetragonal ZrO_2 and accelerates the water–gas shift reverse reaction in the Ni/ZrO_2–CeO_2 catalyst, which helps to reduce carbon deposition [45].

Thus, nickel catalysts are suitable for eliminating the use of noble metals and can be used for both carbon dioxide reforming and methane partial oxidation [46]. They usually strike a good balance between performance and cost. Therefore, much attention is paid to the development of new improved catalytic systems with a relatively low cost.

The aim of the work is to develop a new efficient catalyst for the dry reforming of methane into synthesis gas, which will further promote the organization of a new and environmentally friendly energy-saving production method.

2. Results and Discussion

2.1. Characterization of Catalysts

The results of our study of catalysts based on a NiO–Al-α-Al_2O_3 system prepared by self-propagating high-temperature synthesis are presented. After combustion, the resulting catalysts were studied by X-ray diffraction (XRD) to establish the formation and identification of phases. The scanning electron microscopy (SEM) method with EDS analysis and Brunauer–Emmett–Teller (BET) analysis were carried out to determine the composition and specific surface area.

At the point of NiO–Al-α-Al_2O_3 combustion in the SHS regime, there are the following processes taking place:

$$Al + Ni \rightarrow NiAl \quad (1)$$

$$2Ni + O_2 \rightarrow 2NiO \quad (2)$$

$$2Al + 3NiO \rightarrow 3Ni + Al_2O_3 \quad (3)$$

$$4Al + 3O_2 \rightarrow 2Al_2O_3 \quad (4)$$

$$Al_2O_3 + NiO \rightarrow NiAl_2O_4 \quad (5)$$

2.1.1. XRD Analysis

The combustion rate was measured during SHS experiments (Table 1). Table 1 also shows the data on X-ray diffraction and specific surface SHS catalysts.

The specific surface areas of catalysts were very low and ranged from 0.3 to 2.1 m^2/g (Table 1). High-temperature combustion, reaching 1500 °C, is the reason for the small surface areas. As shown in earlier works, SHS catalysts have a high specific activity, which even allows them to compete with platinum-group catalysts with a large surface area. The optimal conditions for the SHS process for each initial composition were determined. SHS will demonstrate an explosive mode if the composition is close to stoichiometric conditions. SHS will not occur if the exothermic effect of the reaction is low. Stable results can only be obtained when the exothermic effect of the reaction is high but not explosive, and when the sample retains its dimensions after combustion (without melting). Al_2O_3 was added to the Al–NiO system as ballast or a carrier to create such conditions.

Figures 1–3 show that NiO–Al–Al_2O_3 catalysts with different ratios of elements have a fairly similar qualitative composition, but they have different phase ratios (Figure 4).

Table 1. The initial batch and catalysts' composition, preheating temperature, combustion rate (V), and surface area (S).

The Initial Batch Composition	T (°C)	V (mm/s)	Catalysts Composition	S (m^2/g)
24.1% NiO—55.9% Al—20.0% Al_2O_3	900	8.75	Al, α-Al_2O_3, NiAl, Ni, NiO, $NiAl_2O_4$	0.3
25.8% NiO—54.2% Al—20.0% Al_2O_3	900	9.07	Al, α-Al_2O_3, NiAl, Ni, NiO, $NiAl_2O_4$	0.3
27.5% NiO—52.5% Al—20.0% Al_2O_3	900	9.12	Al, α-Al_2O_3, NiAl, Ni, NiO, $NiAl_2O_4$	0.32
29.2% NiO—50.8% Al—20.0% Al_2O_3	900	9.25	Al, α-Al_2O_3, NiAl, Ni, NiO, $NiAl_2O_4$	0.35
31.0% NiO—49.0% Al—20.0% Al_2O_3	850	9.42	Al, α-Al_2O_3, NiAl, Ni, NiO, $NiAl_2O_4$	0.4
34.4% NiO—45.6% Al—20.0% Al_2O_3	800	9.83	Al, α-Al_2O_3, NiAl, Ni, NiO, $NiAl_2O_4$	0.48
31.0% NiO—19.0% Al—50.0% Al_2O_3	900	9.15	Al, α-Al_2O_3, NiAl, Ni, NiO, $NiAl_2O_4$	0.8
28.0% NiO—42.0% Al—30.0% Al_2O_3	800	9.17	Al, α-Al_2O_3, NiAl, Ni, NiO, $NiAl_2O_4$	0.5
39.0% NiO—10.0% Al—30.0% Al_2O_3 7.0% Mg—14.0% MgO_2	850	7.42	$MgAl_2O_4$, $NiAl_2O_4$, NiAl, $MgNiO_2$, NiO, MgO, Ni	1.7
87.0% NiO—12.6% Al—0.4% H_3BO_3	650	8.17	Al_2O_3, Ni, NiO, Al, $AlBO_3$, $NiAl_2O_4$	2.1
10.0% NiO—28.0% Al—40.0% Al_2O_3 22.0% MoO_3	900	12.48	Al, Al_2O_3, MoO, MoO_2, Al_3Mo, $NiAl_2O_4$	1.4

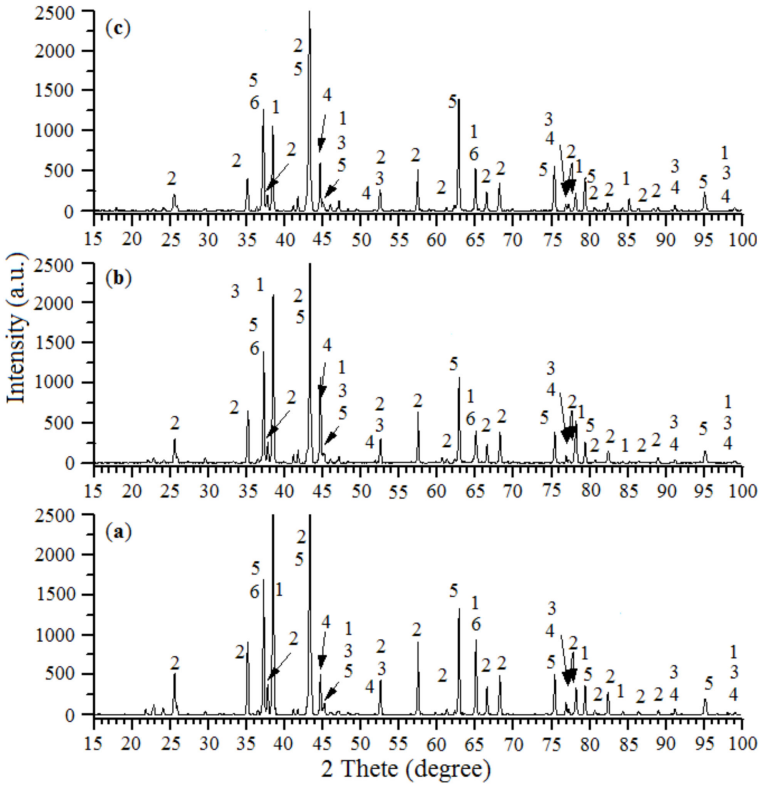

Figure 1. XRD analysis of the NiO–Al–Al_2O_3 catalysts with different contents of elements: (**a**) 29.2% NiO—50.8% Al—20.0% Al_2O_3, (**b**) 31.0% NiO—49.0% Al—20.0% Al_2O_3, (**c**) 34.4% NiO—45.6% Al—20.0% Al_2O_3. Note: 1—Al, 2—α-Al_2O_3, 3—NiAl, 4—Ni, 5—NiO, 6—$NiAl_2O_4$.

Figure 3 shows the X-ray diffraction spectrums for NiO–Al–Al_2O_3 with A catalysts (where A—H_3BO_3, MgO_2, MoO_3).

Figures 4 and 5 show the detected phases and the relationships between them, which were determined from the relative intensity of the X-ray diffraction peaks. The maximum formation of NiAl and $NiAl_2O_4$ phases was observed at a content of 52–53% Al and 26–27% NiO.

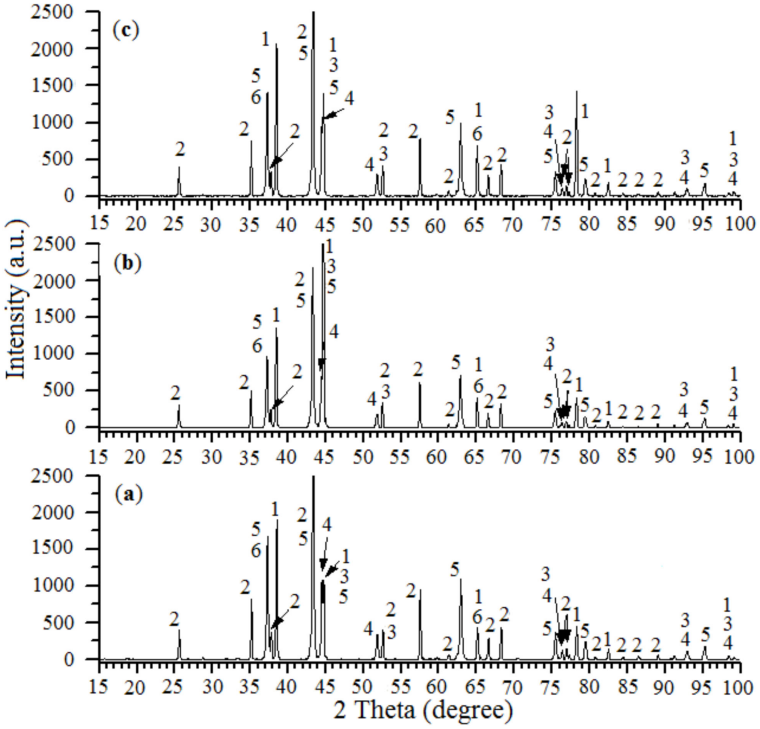

Figure 2. XRD analysis of the NiO–Al–Al_2O_3 catalysts with different content of elements: (**a**) 24.1% NiO—55.9% Al—20.0% Al_2O_3, (**b**) 25.8% NiO, 54.2% Al—20.0% Al_2O_3, (**c**) 27.5% NiO—52.5% Al—20.0% Al_2O_3. Note: 1—Al, 2—α-Al_2O_3, 3—NiAl, 4—Ni, 5—NiO, 6—$NiAl_2O_4$.

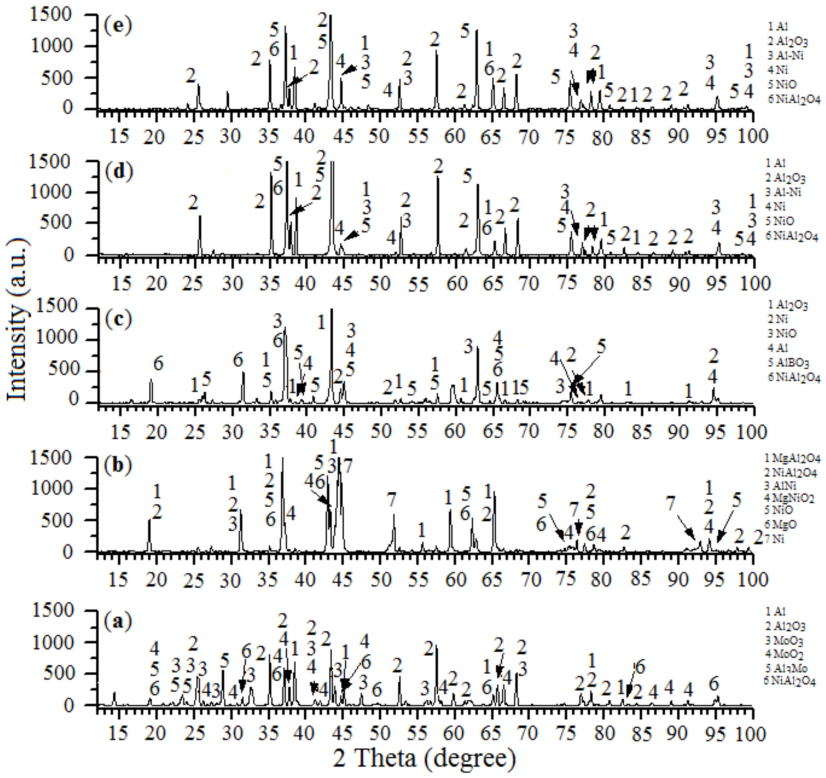

Figure 3. XRD analysis of the NiO–Al–Al_2O_3 with the addition of H_3BO_3, MgO_2, MoO_3 and different contents of elements: (**a**) 10.0% NiO—28.0% Al—40.0% Al_2O_3—22.0% MoO_3, (**b**) 39.0% NiO—10.0% Al—30.0% Al_2O_3—7.0% Mg—14.0% MgO, (**c**) 87.0% NiO—12.6% Al—0.4% H_3BO_3, (**d**) 31.0% NiO—19.0% Al—50.0% Al_2O_3, (**e**) 28.0% NiO—42.0% Al—30.0% Al_2O_3.

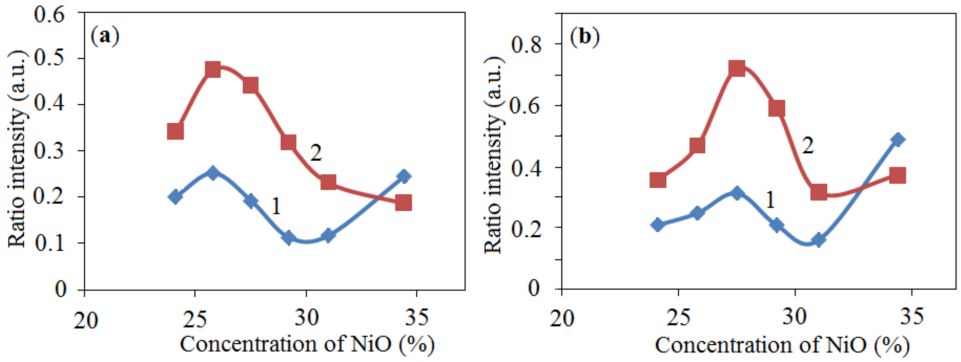

Figure 4. The influence of the NiO content in NiO–Al–Al_2O_3 catalysts on the phase ratio: (**a**) 1—NiAl/Al, 2—NiAl/NiO; (**b**) 1—$NiAl_2O_4$/Al, 2—$NiAl_2O_4$/NiO.

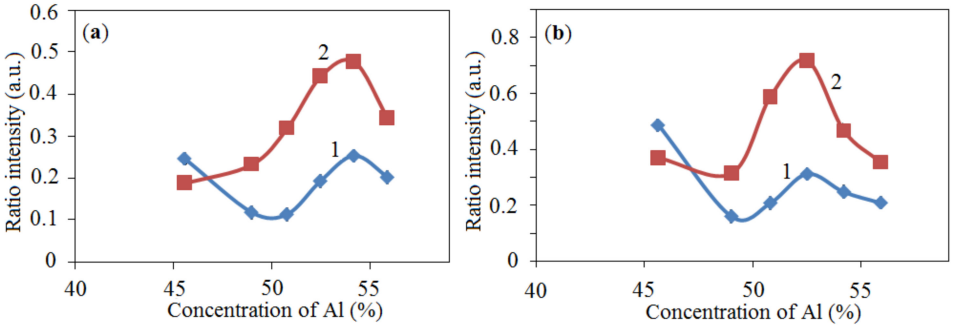

Figure 5. The influence of the Al content in NiO–Al–Al_2O_3 catalysts on the phase ratio: (**a**) 1—NiAl/Al, 2—NiAl/NiO; (**b**) 1—$NiAl_2O_4$/Al, 2—$NiAl_2O_4$/NiO.

Thus, varying the contents of elements in the composition of catalysts leads to a change in the phase ratio of the products formed by the SHS reaction (Figures 4 and 5).

The dependence of the combustion rate on the initial catalyst composition is shown in Figure 6.

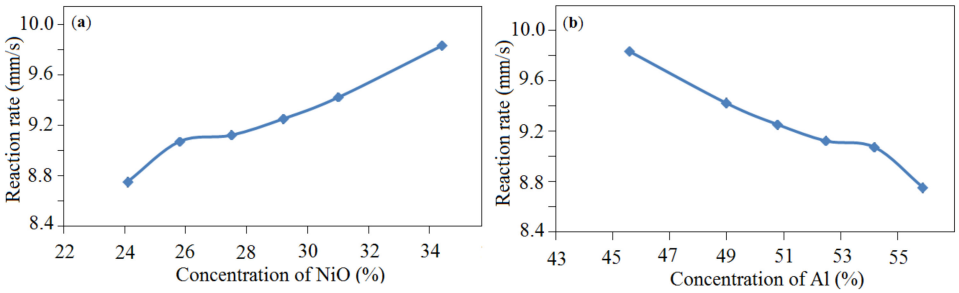

Figure 6. Effect of the catalyst composition on the combustion rate during SHS: (**a**) NiO, (**b**) Al.

Increasing the concentration of NiO and decreasing the concentration of Al in the composition of catalysts leads to an increase in the combustion rate (Figure 6). Apparently, this effect can be explained by approaching the stoichiometric composition, which results in a large heat release. This increases the rate of the reaction.

Interestingly, the maximum yield of products (Figures 4 and 5) is not observed at the highest temperatures (Figure 6) due to the fact that at higher temperatures, the metal is rapidly oxidized, and, accordingly, the yield of intermetallic compounds decreases. High temperatures (when the initial charge contains more than 27% nickel oxide and less than 55% aluminum) affect the stabilization of the crystal lattice, as can be seen in Figure 7.

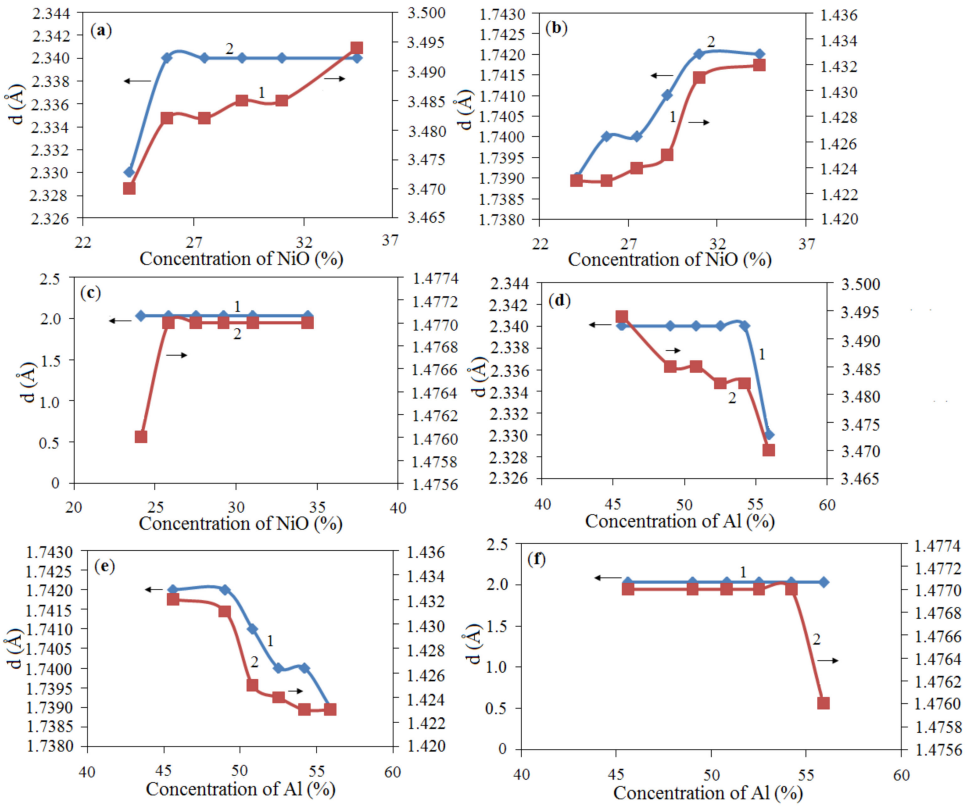

Figure 7. Influence of the catalyst composition on the crystal lattice parameters of the SHS catalyst: (**a**) 1—Al_2O_3, 2—Al; (**b**) 1—$NiAl_2O_4$, 2—NiAl; (**c**) 1—Ni, 2—NiO; (**d**) 1—Al, 2—Al_2O_3; (**e**) 1—NiAl, 2—$NiAl_2O_4$; (**f**) 1—Ni, 2—NiO. The arrow points to the coordinate axis.

Thus, it was found that changing the parameters of the crystal lattice will affect the catalytic activity.

2.1.2. Investigation of the Structure and Composition of SHS Catalysts Using a Scanning Electron Microscope with Chemical Analysis

The phase composition and structures of SHS catalysts (NiO content of 24.1 and 34.4 wt % in the initial catalyst mixture) were studied using a scanning electron microscope. It was established by chemical analysis that the phase composition (Al, α-Al_2O_3, NiAl, Ni, NiO, $NiAl_2O_4$) corresponds to the XRD data. The results of the analysis of catalyst composition (24.1% NiO—55.9% Al—20% Al_2O_3) are shown in Figure 8. Chemical analysis (see Figure 9) was carried out for the area indicated in the image (EDS 1) or at the point (EDS 2) (see Figure 8).

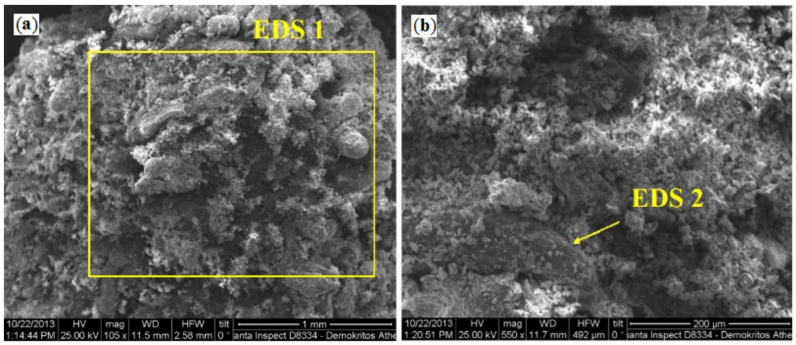

Figure 8. SEM images of the 24.1% NiO—55.9% Al—20.0% Al_2O_3 catalyst after 900 °C treatment: (**a**) sample with area indicated in the image (EDS 1) at 1 μm scale; (**b**) sample with point (EDS 2) at 200 μm scale.

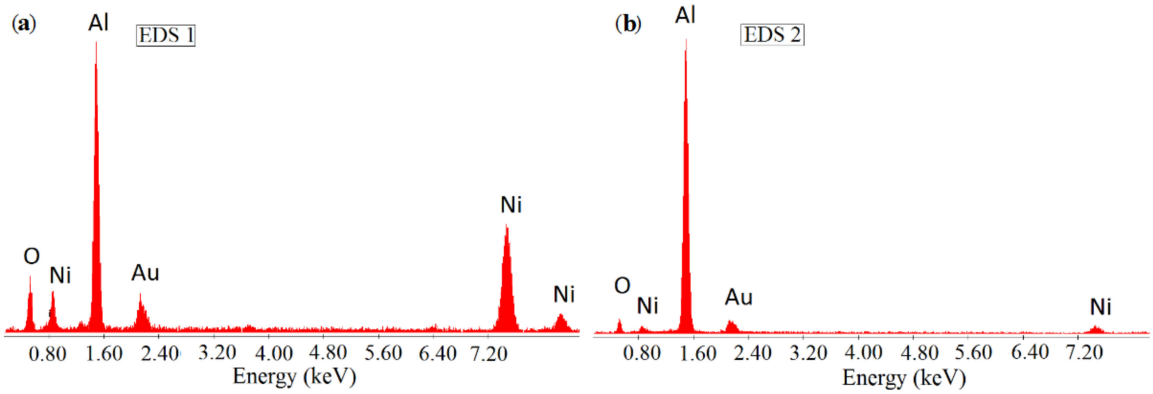

Figure 9. Chemical analysis of the 24.1% NiO—55.9% Al—20% Al_2O_3 catalyst: (**a**) for the area (EDS 1); (**b**) for the point (EDS 2).

The contents of nickel, aluminum, and oxygen vary in different areas of the catalyst (Figure 9). A sufficiently high content of nickel, aluminum, and oxygen corresponds to the spinel phase. The NiAl phase was determined to be at a high content of nickel and aluminum and with an almost complete absence of oxygen. SEM images of the 34.4% NiO—45.6% Al—20% Al_2O_3 catalyst are shown in Figure 10.

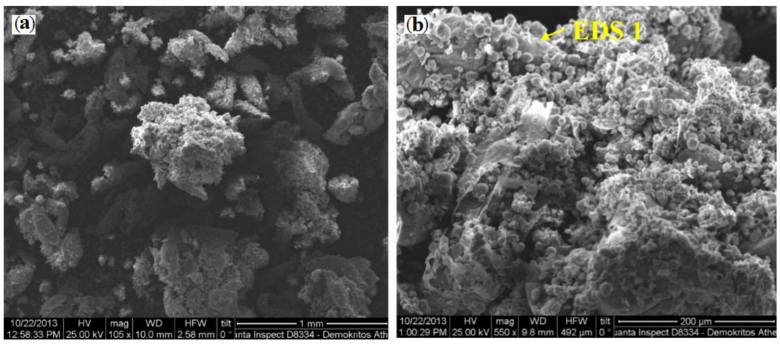

Figure 10. SEM images of the 34.4% NiO—45.6% Al—20% Al_2O_3 catalyst after 900 °C treatment: (**a**) sample at 1 μm scale; (**b**) sample at 200 μm scale.

Chemical analysis (Figure 11) was carried out in the area indicated in Figure 10.

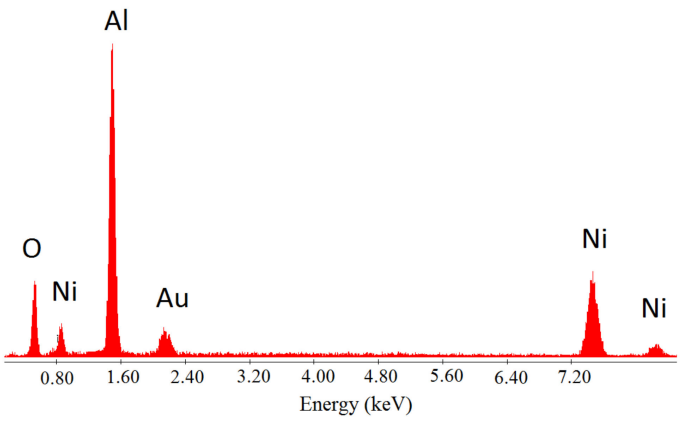

Figure 11. Chemical analysis of the 34.4% NiO—45.6% Al—20% Al_2O_3 catalyst.

Thus, NiO–Al-α-Al_2O_3 catalysts with various element ratios were synthesized, their combustion characteristics, composition, and structure of the resulting catalysts, and their specific surface were studied.

2.2. Catalytic Results

2.2.1. Dry Reforming of Methane

A series of synthesized SHS catalysts was studied in the dry reforming of methane at 750–900 °C. Figure 12 shows the results of methane and CO_2 conversion, product yields, and H_2/CO ratios for the studied NiO–Al-α-Al_2O_3 catalysts.

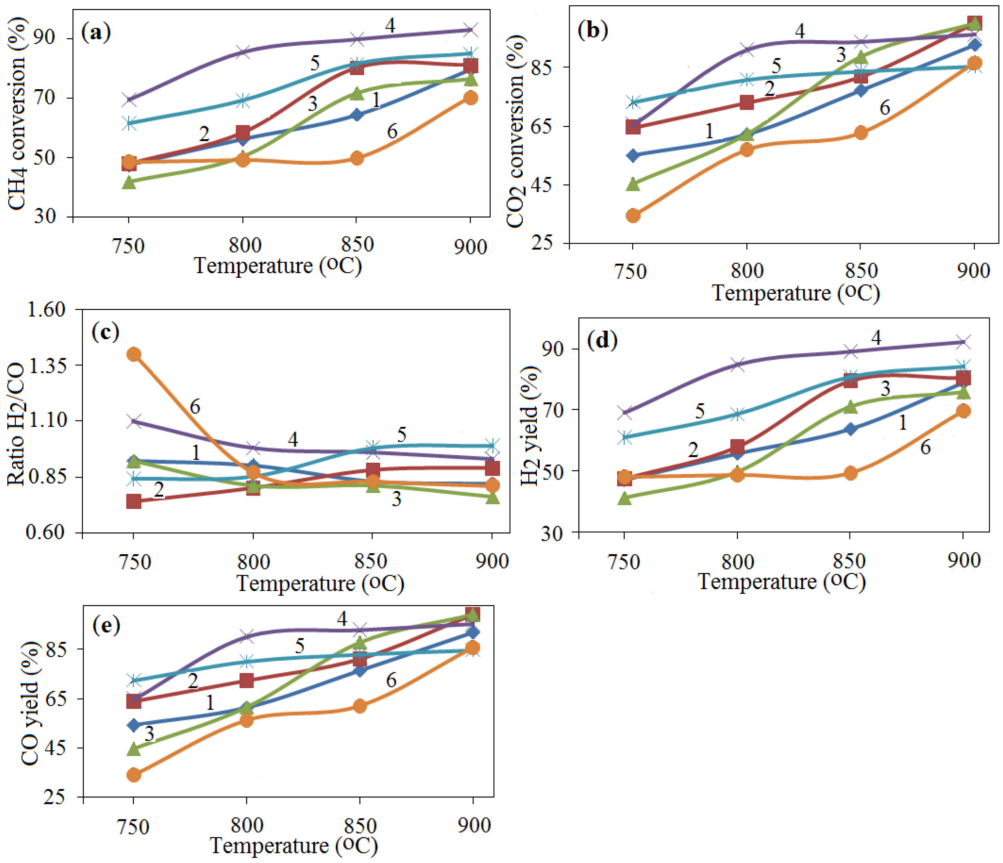

Figure 12. Dry reforming of methane on NiO–Al-Al_2O_3 catalysts with different ratios of elements: 1—24.1% NiO—55.9% Al—20% Al_2O_3 (▬), 2—25.8% NiO—54.2% Al + 20% Al_2O_3 (▬), 3—27.5% NiO—52.5% Al—20% Al_2O_3 (▬), 4—29.2% NiO—50.8% Al—20% Al_2O_3 (▬), 5—31% NiO—49% Al—20% Al_2O_3 (▬), 6—34.4% NiO—45.6% Al—20% Al_2O_3 (▬); (**a**) CH_4 conversion, (**b**) CO_2 conversion, (**c**) H_2/CO ratio, (**d**) H_2 yield, (**e**) CO yield; GHSV—860 h^{-1}.

In summary, 93% CH_4 conversion, 99% CO_2 conversion, 92% H_2 yield, and 99% CO yield are the best results achieved for SHS catalysts based on NiO–Al–Al_2O_3 (Figure 12). The H_2/CO ratio varies in the range of 0.7–1.35. The increase in the H_2/CO ratio with an increase in the reaction temperature is most likely due to the intensification of the dehydrogenation reaction.

Figure 13 shows the results of the dry reforming of methane on SHS catalysts, based on NiO–Al–Al_2O_3–MoO_3, Al–NiO–H_3BO_3, and Al–Mg–NiO–Al_2O_3–MgO_2 (for comparison, a catalyst based on NiO–Al–Al_2O_3 is also shown).

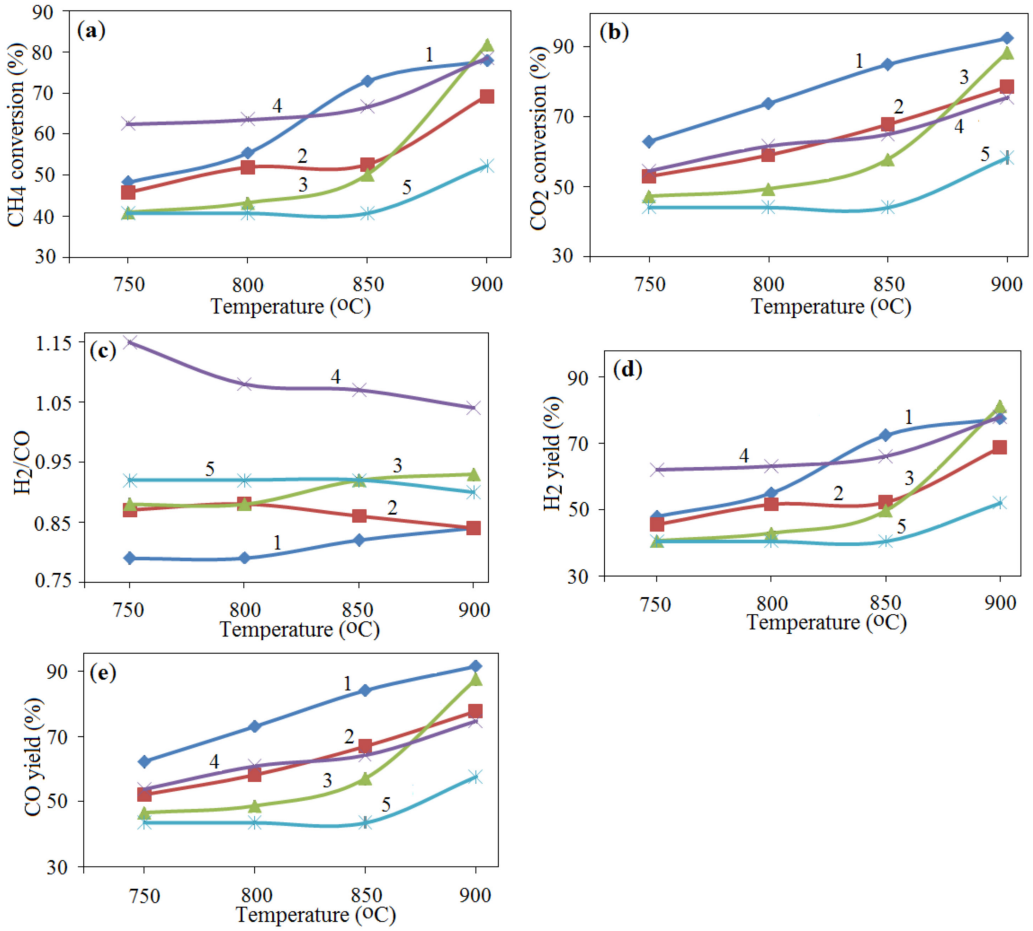

Figure 13. Dry reforming of methane on NiO–Al-Al_2O_3 catalysts with different ratios of elements: 1—31% NiO—19% Al—50% Al_2O_3 (—), 2—28% NiO—42% Al—30% Al_2O_3 (—), 3—39% NiO—10% Al—30% Al_2O_3—7% Mg—14% MgO_2 (—), 4—7% NiO—12.6% Al—0.4% H_3BO_3 (—), 5—10% NiO—28% Al—40% Al_2O_3—22% MoO_3 (—); (**a**)—CH_4 conversion, (**b**)—CO_2 conversion, (**c**)—H_2/CO ratio, (**d**)—H_2 yield, (**e**)—CO yield, GHSV—860 h^{-1}.

Figure 13 shows the best results for catalysts based on NiO–Al–Al_2O_3-M (M—MoO_3, H_3BO_3, MgO_2): CH_4 conversion—80%, CO_2 conversion—2%, product yield—80% H_2 and 90% CO. The H_2/CO ratio in the reaction products ranges from 0.78 to 1.15. Increasing the reaction temperature usually results in an increase in the H_2/CO ratio due to the additional dehydrogenation reaction. Thus, additions to the NiO–Al–Al_2O_3 catalyst did not lead to positive results.

Figure 14 shows the dependence of methane and carbon dioxide conversion and the H_2/CO ratio on the concentrations of aluminum and nickel oxide in the initial charge.

Figure 14 shows the effect of aluminum concentration in the catalyst composition on CH_4 and CO_2 conversion, as well as on the H_2/CO ratio. It can be seen that 51% aluminum content in the initial batch is optimal for obtaining the maximum hydrogen yield, while 51–56% aluminum in the catalyst composition is necessary to obtain high CO yields.

The content of nickel oxide in the composition of the catalyst plays an important role in relation to the conversion of CH_4 and CO_2, as well as to the H_2/CO ratio, since the content of nickel spinel, the active component of the catalyst, depends on the concentrations of nickel oxide.

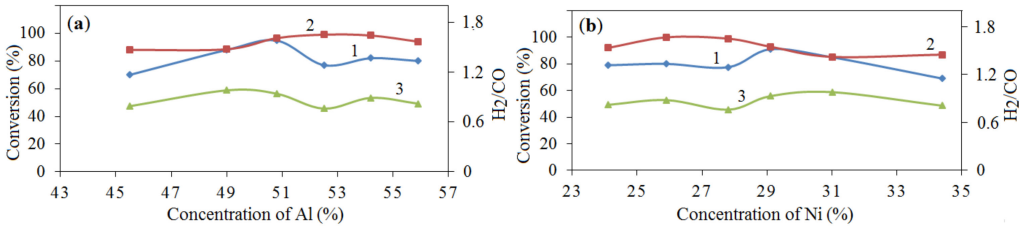

Figure 14. Effect of the content of Al and Ni in the composition of the catalyst on the conversion of CH_4 and CO_2, as well as the H_2/CO ratio: (**a**) Al, (**b**) Ni. Note: 1—CH_4 conversion, 2—CO_2 conversion, 3—H_2/CO ratio. T = 900 °C.

The use of 24–30% nickel oxide in the catalyst mixture leads to the high conversion of carbon dioxide. It is possible to achieve maximum CH_4 conversion at 29% NiO content in the catalyst. A clear effect of the contents of aluminum and NiO in the composition of the initial batch on the H_2/CO ratio was not found.

Taking into account the results presented in Figures 4 and 5 on the effect of the contents of NiO and Al on the phase state, as well as the data regarding dry methane reforming, it was possible to establish that the maximum amount of $NiAl_2O_4$ and NiAl was found in the catalyst with 51% aluminum and 29% nickel oxide.

Figure 15 shows the dependence of CH_4 and CO_2 conversion, as well as the H_2/CO ratio, on structural deformation and catalyst composition.

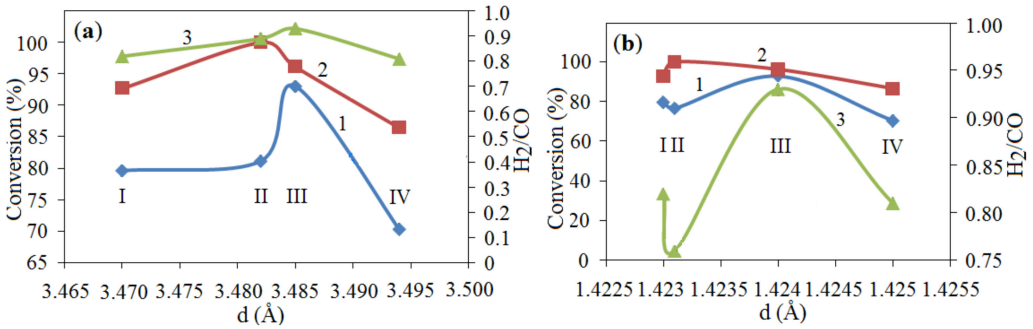

Figure 15. Effect of structural deformation and the composition of catalysts on CH_4 and CO_2 conversion and on the H_2/CO ratio: (**a**) Al_2O_3: I—24.1% NiO, II—25.8% NiO, III—29.2% NiO, IV—34.4% NiO; (**b**) $NiAl_2O_4$: I—24.1% NiO, II—27.5% NiO, III—29.2% NiO, IV—34.4% NiO. Note: 1—CH_4 conversion, %, 2—CO_2 conversion, %, 3—H_2/CO ratio. T = 900 °C.

These data indicate a clear dependence of the catalyst activity on structural deformation. They also show that 3.48–3.485 Å for alumina and 1.42 Å for $NiAl_2O_4$ are the optimal lattice parameters for the maximum conversion of carbon dioxide and methane.

The weight of the catalysts did not change after catalytic studies, which indicates the absence of coke formation. The stability of the catalysts has been investigated over 70 h, the results of which are shown in Figure 16. The conversion of both CH_4 and CO_2 fluctuated slightly during the entire study period. Further and more in-depth studies on coke formation are currently being carried out.

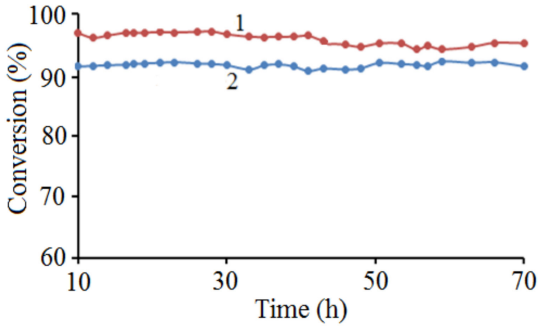

Figure 16. Influence of the duration of the experiment on the stability of the catalyst. Note: 1—CO_2 conversion, %, 2—CH_4 conversion.

Carbon can be formed by the methane dissociation reaction (6) and the Boudouard reaction (7) during methane reforming:

$$CH_4 \rightarrow C + 2H_2 \quad (6)$$

$$2CO \rightarrow C + CO_2 \quad (7)$$

These reactions will take place to a greater or lesser extent in any case. Removal of carbon deposits can be carried out as a result of the gasification reaction (8) and the reverse Boudouard reaction (9):

$$C + H_2O \rightarrow H_2 + CO \quad (8)$$

$$CO_2 + C \rightarrow 2CO \quad (9)$$

According to the data [47–49] and the results obtained by the authors in further studies, it can be assumed that the uniqueness of the configuration, the size of the crystal lattice, and high dispersion improve the characteristics of the catalysts. Moreover, the SHS method should be especially noted, as a result of which highly dispersed samples are obtained. In addition, the small size of Ni crystallites ($\leq$ 10 nm), dispersion and higher basicity increase not only the activity but also the stability of the catalysts. Deeper studies of the influence of both the above and a number of other factors make it possible to find suitable conditions for the implementation of process with the lowest possible carbon deposition on catalyst surface.

The SHS catalysts were compared with samples of the same composition, prepared using the impregnation method. Catalysts of the following compositions: 24.1% NiO—55% Al—20% Al_2O_3, 25.7% NiO—54.2% Al—20% Al_2O_3, 27.5% NiO—52.5% Al—20% Al_2O_3, 29.2% NiO—50.8% Al—20% Al_2O_3 were prepared by the impregnation method. The dry reforming of methane was carried out in the reaction mixture of CH_4:CO_2:Ar = 1:1:1 at a space velocity GHSV of 860 h^{-1}. Figure 17 presents the results of the study. Methane and CO conversion values are close for the SHS catalysts and for samples prepared by the impregnation method. The H_2 yield is higher for SHS catalysts and is at 80%, compared to 48–51% for the supported catalysts. The yield of CO reached 40–42% on the supported catalysts and about 90% on the SHS samples. Thus, new composite materials prepared by the SHS method have a significant advantage. The resulting mixture of hydrogen and CO is pure and does not require additional purification.

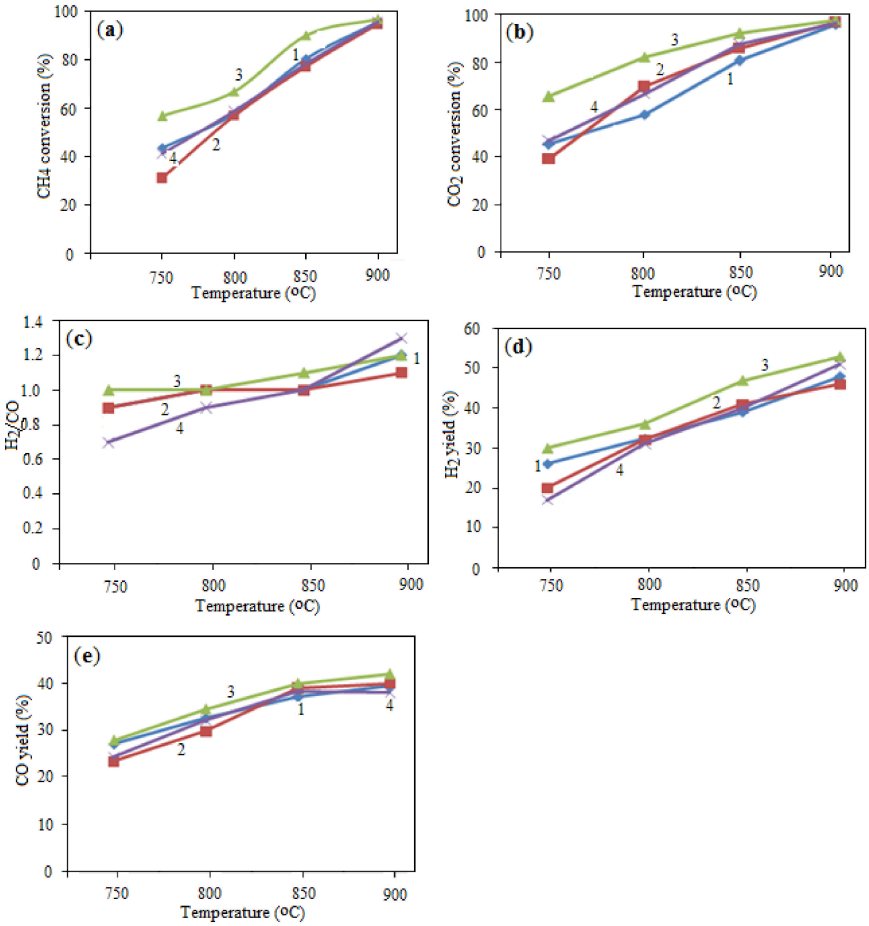

Figure 17. The dry reforming of methane on NiO–Al–Al_2O_3 catalysts prepared by the impregnation method. (**a**) CH_4 conversion, (**b**) CO_2 conversion, (**c**) H_2/CO ratio, (**d**) H_2 yield, (**e**) CO yield, GHSV—860 h^{-1}. Note: 1—24.1% NiO—55.9% Al—20% Al_2O_3, 2—25.8% NiO—54.2% Al—20% Al_2O_3, 3—27.5% NiO—52.5% Al—20% Al_2O_3, 4—29.2% NiO—50.8% Al—20% Al_2O_3.

2.2.2. Partial Oxidation of Methane

The partial oxidation of methane was carried out in a reaction mixture of the following composition: 34% CH_4—17% O_2—50% Ar, at a space velocity of 2500 h^{-1}. For these tests, NiO–Al-α-Al_2O_3 catalysts prepared using the SHS method and the traditional impregnation method were used (Table 2).

Table 2. Oxidative conversion of CH_4 on the NiO–Al-α-Al_2O_3 catalysts prepared using the SHS and impregnation methods.

The Initial Batch Composition	CH_4 Conversion (%)		H_2 Yield (%)		CO Yield (%)		H_2/CO	
	SHS	IM	SHS	IM	SHS	IM	SHS	IM
24.1% NiO—55.9% Al—20% Al_2O_3	90	78.8	61.5	54.9	21	21.9	2.9	2.5
25.8% NiO—54.2% Al—20% Al_2O_3	84.2	66.9	62	57.2	26.4	22.4	2.3	2.6
27.5% NiO—52.5% Al—20% Al_2O_3	96	69.4	67	53.9	27.1	24.2	2.5	2.2
29.2% NiO—50.8% Al—20% Al_2O_3	81.7	73.7	52	55.7	25.9	22.8	2	2.4

A higher conversion rate was observed with SHS catalysts in the partial oxidation of methane (81.7–96.0%), compared to the impregnation catalysts (66.9–78.8%). The same dependence is presented: for hydrogen yields—SHS catalysts (52.0–67.0%) and supported samples (53.9–57.2%); for CO yields—SHS catalysts (21.0–27.1%) and supported samples (21.9–24.2%). The H_2/CO ratio varied between 2.0 and 2.9. The most suitable ratio for

further syntheses, $H_2/CO = 2$, was obtained for the SHS catalysts (29.2% NiO—50.8% Al—20% Al_2O_3).

3. Materials and Methods

3.1. Catalysts Preparation and Characterization

SHS catalysts from the initial charge of NiO–Al-α-Al_2O_3 were prepared from aluminum, aluminum oxide, and nickel oxide at a preheating temperature of 650–900 °C. Uniaxial pressing under a pressure of about 10 MPa was used to prepare cylindrical specimens that were 10 mm in diameter and 20 mm long. The initial reaction mixture was preliminarily heated in a muffle furnace at a temperature of 700–900 °C for 3–5 min before initiating the SHS reaction.

Catalysts of the same composition were prepared by the impregnation method. α-Al_2O_3, with a granule size of 100–200 μm and a surface area of 57.7 m^2/g, was impregnated with an aqueous solution of nickel nitrate, heated in air at 250 °C for 5 h and at 600 °C for 2 h, then calcined at 900 °C for 1 h. Metal nitrate salts (purity 98–99%) were purchased from Sigma-Aldrich (Darmstadt, Germany), and high-purity alumina from the Angarsk Chemical Reagents Plant (Angarsk, Russia).

The synthesized catalysts were characterized by XRD, SEM, and EDS methods, as described in [46]. The BET method was used to determine the surface area of the catalysts [46].

Source gases and reaction products were analyzed on two chromatographs for accuracy control: first, on a gas chromatograph with a 10-m-long steel column filled with Highset-d polymer at 40 °C, using He as a carrier gas and a flame ionization detector. Second, an Agilent 6890N gas chromatograph (Agilent Technologies, Singapore Pte. Ltd., Singapore) with software equipped with a flame ionization detector and a thermal conductivity detector was used for the on-line analysis of the starting materials and reaction products. The feed gas mixture and the reaction products were analyzed with a copper capillary column HP-PLOT Q of 30 m long and 0.53 mm in diameter, filled with polystyrene-divinylbenzene.

3.2. Catalytic Reaction

The catalytic activity of the prepared catalysts was determined in the process of the dry reforming of methane. For this purpose, coarsely ground samples with an average granule size of 3 mm were used, which is determined by the needs of production. The tests were carried out in a flow-through quartz reactor with a fixed catalyst bed at a ratio of reaction components of CO_2:CH_4:Ar = 1:1:1, at atmospheric pressure, for the dry reforming of methane. Then, a 34% CH_4—17% O_2—50% Ar reaction mixture was used for the partial oxidation of methane at 900 °C and at a space velocity of 2500 h^{-1}. The catalyst was placed in the central part of the reactor and quartz wool was placed above and below the catalyst bed. The reaction was carried out at 700–900 °C and at a space velocity of 860 h^{-1} and 3300 h^{-1} for the dry reforming of methane.

4. Conclusions

For this study, Al–NiO–Al_2O_3 catalysts were prepared using both SHS and impregnation methods for research into the processes of the dry reforming of methane and partial oxidation of methane, and studies of their properties and activity in the above reactions were carried out. As a result of these studies of Al–NiO–Al_2O_3 catalysts, using a complex of XRD, SEM, and BET methods, data were obtained for understanding the catalytic activity of catalysts in the processes of the oxidative conversion of methane into synthesis gas. The reasons for the optimal activity of the catalyst have been established.

Increasing the concentration of NiO and decreasing the concentration of Al in the composition of catalysts leads to an increase in the combustion rate. Apparently, this effect can be explained by approaching the stoichiometric composition, which results in a large heat release. High temperatures (when the initial charge contains more than 27% of nickel

oxide and less than 55% of aluminum) affect the stability of the crystal lattice. Changing the parameters of the crystal lattice will affect the catalytic activity. It can be seen from the findings that 93% CH_4 conversion, 99% CO_2 conversion, 92% H_2 yield, and 99% CO yield are the best results for SHS catalysts based on NiO–Al–Al_2O_3. The H_2/CO ratio varies in the range of 0.7–1.35. The maximum amount of $NiAl_2O_4$ and NiAl was found in the catalyst with 51% aluminum and 29% nickel oxide. We have also ascertained that 3.48–3.485 Å for alumina and 1.42 Å for $NiAl_2O_4$ are the optimal lattice parameters for the maximum conversion of carbon dioxide and methane.

Author Contributions: Conceptualization, S.T. and G.X.; methodology, G.V.; validation, T.B. and M.S.; formal analysis, M.Z.; investigation, K.K.; data curation, T.B.; writing—original draft preparation, S.T.; writing—review and editing, G.X.; supervision, M.Z. All authors have read and agreed to the published version of the manuscript.

Funding: This research was funded by the Science Committee of the Ministry of Education and Science of the Republic of Kazakhstan, grant number AP08855562.

Data Availability Statement: The data presented in this study are available upon request from the corresponding author.

Acknowledgments: The authors are especially grateful to the staff of the Laboratory of Physical and Chemical Research Methods.

Conflicts of Interest: The authors declare no conflict of interest. The funders had no role in the design of the study; in the collection, analyses, or interpretation of data; in the writing of the manuscript; or in the decision to publish the results.

References

1. Fouquet, R. Historical energy transitions: Speed, prices and system transformation. *Energy Res. Soc. Sci* **2016**, *22*, 7–12. [CrossRef]
2. Davidson, D.J. Exnovating for a renewable energy transition. *Nat. Energy* **2019**, *4*, 254–256. [CrossRef]
3. Allen, M.R.; Frame, D.J.; Huntingford, C.; Jones, C.D.; Lowe, J.A.; Meinshausen, M.; Meinshausen, N. Warming caused by cumulative carbon emissions towards the trillionth tonne. *Nature* **2009**, *458*, 1163–1166. [CrossRef]
4. Matthews, H.D.; Gillett, N.P.; Stott, P.A.; Zickfeld, K. The proportionality of global warming to cumulative carbon emissions. *Nature* **2009**, *459*, 829–832. [CrossRef]
5. Hakawati, R.; Smyth, B.M.; McCullough, G.; De Rosa, F.; Rooney, D. What is the most energy efficient route for biogas utilization: Heat, electricity or transport? *Appl. Energy* **2017**, *206*, 1076–1087. [CrossRef]
6. Iyer, M.V.; Norcio, L.P.; Kugler, E.L.; Dadyburjor, D.B. Kinetic modeling for methane reforming with carbon dioxide over a mixed-metal carbide catalyst. *Ind. Eng. Chem. Res.* **2003**, *42*, 2712–2721. [CrossRef]
7. Barrai, F.; Jackson, T.; Whitmore, N.; Castaldi, M. The role of carbon deposition on precious metal catalyst activity during dry reforming of biogas. *Catal. Today* **2007**, *129*, 391–396. [CrossRef]
8. Kohn, M.P.; Castaldi, M.J.; Farrauto, R.J. Auto-thermal and dry reforming of landfill gas over a Rh/γAl_2O_3 monolith catalyst. *Appl. Catal. B* **2010**, *94*, 125–133. [CrossRef]
9. Lu, S.-M. A global survey of gas hydrate development and reserves: Specifically in the marine field. *Renew. Sustain. Energy Rev.* **2015**, *41*, 884–900. [CrossRef]
10. *Statistical Review of World Energy*, 69th ed.; BP p.l.c.: London, UK, 2020; p. 65. Available online: https://www.bp.com/content/dam/bp/business-sites/en/global/corporate/pdfs/energy-economics/statistical-review/bp-stats-review-2020-full-report.pdf (accessed on 10 September 2022).
11. Danghyan, V.; Kumar, A.; Mukasyan, A.; Wolf, E.E. An active and stable NiOMgO solid solution based catalysts prepared by paper assisted combustion synthesis for the dry reforming of methane. *Appl. Catal. B* **2020**, *273*, 119056. [CrossRef]
12. Ghareghashi, A.; Shahraki, F.; Razzaghi, K.; Ghader, S.; Torangi, M.A. Enhancement of gasoline selectivity in combined reactor system consisting of steam reforming of methane and Fischer-Tropsch synthesis. *Korean J. Chem. Eng.* **2017**, *34*, 87–99. [CrossRef]
13. Monteiro, W.F.; Vieira, M.O.; Calgaro, C.O.; Perez-Lopez, O.W.; Ligabue, R.A. Dry reforming of methane using modified sodium and protonated titanate nanotube catalysts. *Fuel* **2019**, *253*, 713–721. [CrossRef]
14. Dedov, A.G.; Loktev, A.S.; Shmigel, A.V.; Tikhonov, P.A.; Lapshin, A.E.; Arsent'ev, M.Y.; Mukhin, I.E.; Ivanov, V.K.; Moiseev, I.I. Selective conversion of methane to synthesis gas: Catalysts based on electrochemically modified nickel foam. *Pet. Chem.* **2017**, *57*, 230–235. [CrossRef]
15. Song, Y.Q.; He, D.H.; Xu, B.Q. Effects of preparation methods of ZrO_2 support on catalytic performances of Ni/ZrO_2 catalysts in methane partial oxidation to syngas. *Appl. Catal. A* **2008**, *337*, 19–28. [CrossRef]
16. Pengpanich, S.; Meeyoo, V.; Rirksomboon, T. Methane partial oxidation over Ni/CeO_2-ZrO_2 mixed oxide solid solution catalysts. *Catal. Today* **2004**, *93*, 95–105. [CrossRef]

17. Matsumura, Y.; Nakamori, T. Steam reforming of methane over nickel catalysts at low reaction temperature. *Appl. Catal. A* **2004**, *258*, 107–114. [CrossRef]
18. Das, S.; Ashok, J.; Bian, Z.; Dewangan, N.; Wai, M.H.; Du, Y. Silica-ceria sandwiched Ni core-shell catalyst for low temperature dry reforming of biogas: Coke resistance and mechanistic insights. *Appl. Catal. B* **2018**, *230*, 220–236. [CrossRef]
19. Souza, G.; Marcilio, N.R.; Perez-Lopez, O.W. Dry reforming of methane at moderate temperatures over modified Co-Al Co-precipitated catalysts. *Mater. Res.* **2014**, *17*, 1047–1055. [CrossRef]
20. La Parola, V.; Pantaleo, G.; Venezia, A. Effects of synthesis on the structural properties and methane partial oxidation activity of Ni/CeO_2 catalyst. *Catalysts* **2018**, *8*, 220. [CrossRef]
21. Luna, A.E.C.; Iriarte, M.E. Carbon dioxide reforming of methane over a metal modified $Ni-Al_2O_3$ catalyst. *Appl. Catal. A* **2008**, *343*, 10–15. [CrossRef]
22. Galanov, S.I.; Kosyreva, K.A.; Litvak, E.A. Partial catalytic oxidation of natural gas to synthesis gas. *Bull. Tomsk. State Univ.* **2012**, *364*, 230–233.
23. Maksimov, Y.M.; Kirdyashkin, A.I.; Arkatova, L.A. Conversion of methane on catalysts obtained via self-propagating high-temperature synthesis. *Catal. Ind.* **2013**, *3*, 245–252. [CrossRef]
24. Fan, X.; Li, L.; Yang, X.; Guo, Z.; Jing, F.; Chu, W. High-performance $Co_xM_{3-x}AlO_y$ (M = Ni, Mn) catalysts derived from microwave-assisted synthesis of hydrotalcite precursors for methane catalytic combustion. *Catal. Today* **2018**, *347*, 23–30. [CrossRef]
25. Merzhanov, A.G.; Borovinskaja, I.P. Historical retrospective of SHS: An autoreview. *Int. J. Self-Propagating High-Temp. Synth.* **2008**, *17*, 242–265. [CrossRef]
26. Mukasyan, A.S.; White, J.D.E. Combustion joining of refractory materials. *Int. J. Self-Propagating High-Temp. Synth.* **2007**, *16*, 154–168. [CrossRef]
27. Manukyan, K.V.; Cross, A.; Roslyakov, S.; Rouvimov, S.; Rogachev, A.S.; Wolf, E.E.; Mukasyan, A.S. Solution combustion synthesis of nano-crystalline metallic materials: Mechanistic studies. *J. Phys. Chem. C* **2013**, *117*, 24417–24427. [CrossRef]
28. Kingsley, J.J.; Patil, K.C. A novel combustion process for the synthesis of fine particle α-alumina and related oxide materials. *Mater. Lett.* **1988**, *6*, 427–432. [CrossRef]
29. Mimani, T.; Patil, K.C. Solution combustion synthesis of nanoscale oxides and their composites. *Mater. Phys. Mech.* **2001**, *4*, 134–137.
30. Liu, Y.; Parisi, J.; Sun, X.; Lei, Y. Solid-state gas sensors for high temperature applications—A review. *J. Mater. Chem. A* **2014**, *2*, 9919–9943. [CrossRef]
31. Jayathilaka, W.A.D.M.; Qi, K.; Qin, Y.; Chinnappan, A.; Serrano-García, W.; Baskar, C.; Ramakrishna, S. Significance of nanomaterials in wearables: A review on wearable actuators and sensors. *Adv. Mater.* **2018**, *31*, 201805921. [CrossRef]
32. Pokhrel, S.; Mädler, L. Flame made particles for sensors, catalysis and energy storage applications. *Energy Fuels* **2020**, *34*, 13209–13224. [CrossRef] [PubMed]
33. Anthony, L.S.; Perumal, V.; Mohamed, N.M.; Saheed, M.S.M.; Gopinath, S.C.B. *Nanomaterials for Healthcare, Energy and Environment*; Advanced Structured Materials; Springer: Berlin/Heidelberg, Germany, 2019; Volume 3, pp. 51–69.
34. Sharma, N.; Ojha, H.; Bharadwaj, A.; Pathak, D.P.; Sharma, R.K. Preparation and catalytic applications of nanomaterials: A review. *RSC Adv.* **2015**, *5*, 53381–53403. [CrossRef]
35. Xin, Y.; Li, S.; Qian, Y.; Zhu, W.; Yuan, H.; Jiang, P.; Wang, L. High-entropy alloys as a platform for catalysis: Progress, challenges, and opportunities. *ACS Catal.* **2020**, *10*, 11280–11306. [CrossRef]
36. Wu, W. Inorganic nanomaterials for printed electronics: A review. *Nanoscale* **2017**, *9*, 7342–7372. [CrossRef]
37. Jin, L.J.; Xie, T.; Ma, B.X.; Li, Y.; Hu, H.Q. Preparation of carbon-$Ni/MgO-Al_2O_3$ composite catalysts for CO_2 reforming of methane. *Int. J. Hydrog. Energy* **2017**, *42*, 5047–5055. [CrossRef]
38. Nair, M.M.; Kaliaguine, S. Structured catalysts for dry reforming of methane. *J. Chem.* **2016**, *40*, 4049–4060.
39. Pashchenko, D. Experimental investigation of synthesis gas production by methane reforming with flue gas over a $NiO-Al_2O_3$ catalyst: Reforming characteristics and pressure drop. *Int. J. Hydrog. Energy* **2019**, *44*, 7073–7082. [CrossRef]
40. González, A.R.; Asencios, Y.J.O.; Assaf, E.M.; Assaf, J.M. Dry reforming of methane on Ni–Mg–Al nano-spheroid oxide catalysts prepared by the sol–gel method from hydrotalcite-like precursors. *Appl. Surf. Sci.* **2013**, *280*, 876–887. [CrossRef]
41. Ali, S.; Khader, M.M.; Almarri, M.J.; Abdelmoneim, A.G. Ni-based Nano-catalysts for the dry reforming of methane. *Catal. Today* **2019**, *343*, 26–37. [CrossRef]
42. Krylov, O.V. Carbon dioxide conversion of methane to synthesis gas. *Russ. J. Gen. Chem.* **2000**, *44*, 19–33.
43. York, A.P.E.; Xiao, T.C.; Green, M.L.H.; Claridge, J.B. Methane oxyforming for synthesis gas production. *Catal. Rev.* **2007**, *49*, 511–560. [CrossRef]
44. Lavoie, J.M. Review on dry reforming of methane, a potentially more environmentally-friendly approach to the increasing natural gas exploitation. *Front. Chem.* **2014**, *2*, 81. [CrossRef] [PubMed]
45. Zhang, X.; Vajglova, Z.; Mäki-Arvela, P.; Peurla, M.; Palonen, H.; Murzin, D.Y.; Tungatarova, S.; Baizhumanova, T.; Aubakirov, Y. Mono- and bimetallic Ni-Co catalysts in dry reforming of methane. *ChemistrySelect* **2021**, *6*, 3424–3434. [CrossRef]
46. Xanthopoulou, G.; Varitis, S.; Zhumabek, M.; Karanasios, K.; Vekinis, G.; Tungatarova, S.A.; Baizhumanova, T.S. Direct reduction of greenhouse gases by continuous dry (CO_2) reforming of methane over Ni-containing SHS catalysts. *Energies* **2021**, *14*, 6078. [CrossRef]

47. Jiménez, J.D.; Betancourt, L.E.; Danielis, M.; Zhang, H.; Zhang, F.; Orozco, I.; Xu, W.; Llorca, J.; Liu, P.; Trovarelli, A.; et al. Identification of highly selective surface pathways for methane dry reforming using mechanochemical synthesis of Pd–CeO_2. *ACS Catal.* **2022**, *12*, 12809–12822. [CrossRef]
48. Shakir, M.; Prasad, M.; Ray, K.; Sengupta, S.; Sinhamahapatra, A.; Liu, S.; Vuthaluru, H.B. $NaBH_4$-assisted synthesis of B–(Ni–Co)/$MgAl_2O_4$ nanostructures for the catalytic dry reforming of methane. *ACS Appl. Nano Mater.* **2022**, *5*, 10951–10961. [CrossRef]
49. Taherian, Z.; Gharahshiran, V.S.; Khataee, A.; Orooji, Y. Synergistic effect of freeze-drying and promoters on the catalytic performance of Ni/MgAl layered double hydroxide. *Fuel* **2022**, *311*, 122620. [CrossRef]